Neuro-Oncology
23(4), 572–585, 2021 | doi:10.1093/neuonc/noaa235 | Advance Access date 17 October 2020

The long noncoding RNA *lnc-HLX-2-7* is oncogenic in Group 3 medulloblastomas

Keisuke Katsushima, Bongyong Lee, Haritha Kunhiraman, Cuncong Zhong, Rabi Murad, Jun Yin, Ben Liu, Alexandra Garancher, Ignacio Gonzalez-Gomez, Hector L. Monforte, Stacie Stapleton, Rajeev Vibhakar, Chetan Bettegowda, Robert J. Wechsler-Reya, George Jallo, Eric Raabe, Charles G. Eberhart, and Ranjan J. Perera

Department of Oncology, Sidney Kimmel Comprehensive Cancer Center, School of Medicine, Johns Hopkins University, Baltimore, Maryland (K.K., B. Lee., H.K., C.B., E.R., C.G.E., R.J.P.); Johns Hopkins All Children's Hospital, Petersburg, Florida (K.K., B. Lee., H.K., I.G-G., H.L.M., S.S., G.J., R.J.P.); University of Kansas, Department of Electrical Engineering and Computer Science, Lawrence, Kansas (C.Z., B. Liu.); Sanford Burnham Prebys Medical Discovery Institute, La Jolla, California (R.M., J.Y., A.G., R.J.W.R., R.J.P.); University of Colorado School of Medicine Center for Cancer and Blood Disorders, Children's Hospital Colorado, Aurora, Colorado (R.V.); Department of Pathology, Johns Hopkins University School of Medicine, Baltimore, Maryland (E.R., C.G.E.)

Corresponding Author: Ranjan J. Perera, PhD, Department of Oncology, Sidney Kimmel Comprehensive Cancer Center, School of Medicine, Johns Hopkins University, 1650 Orleans St., Baltimore, MD 21231 (jperera2@jh.edu).

Abstract

Background. Medulloblastoma (MB) is an aggressive brain tumor that predominantly affects children. Recent high-throughput sequencing studies suggest that the noncoding RNA genome, in particular long noncoding RNAs (lncRNAs), contributes to MB subgrouping. Here we report the identification of a novel lncRNA, *lnc-HLX-2-7*, as a potential molecular marker and therapeutic target in Group 3 MBs.

Methods. Publicly available RNA sequencing (RNA-seq) data from 175 MB patients were interrogated to identify lncRNAs that differentiate between MB subgroups. After characterizing a subset of differentially expressed lncRNAs in vitro and in vivo, *lnc-HLX-2-7* was deleted by CRISPR/Cas9 in the MB cell line. Intracranial injected tumors were further characterized by bulk and single-cell RNA-seq.

Results. *Lnc-HLX-2-7* is highly upregulated in Group 3 MB cell lines, patient-derived xenografts, and primary MBs compared with other MB subgroups as assessed by quantitative real-time, RNA-seq, and RNA fluorescence in situ hybridization. Depletion of *lnc-HLX-2-7* significantly reduced cell proliferation and 3D colony formation and induced apoptosis. *Lnc-HLX-2-7*–deleted cells injected into mouse cerebellums produced smaller tumors than those derived from parental cells. Pathway analysis revealed that *lnc-HLX-2-7* modulated oxidative phosphorylation, mitochondrial dysfunction, and sirtuin signaling pathways. The *MYC* oncogene regulated *lnc-HLX-2-7*, and the small-molecule **bromodomain** and extraterminal domain family–bromodomain 4 inhibitor Jun Qi 1 (JQ1) reduced *lnc-HLX-2-7* expression.

Conclusions. *Lnc-HLX-2-7* is oncogenic in MB and represents a promising novel molecular marker and a potential therapeutic target in Group 3 MBs.

Key Points

1. *Lnc-HLX-2-7* is highly upregulated in Group 3 MB compared with other subgroups.
2. In vitro and in vivo studies strongly support an oncogenic role for *lnc-HLX-2-7* in Group 3 MB.
3. *Lnc-HLX-2-7* may be a novel biomarker and a potential therapeutic target in Group 3 MB.

Importance of the Study

Group 3 MBs are associated with poor clinical outcomes, are difficult to subtype clinically, and have a biology that is poorly understood. In an effort to address these problems, we identified a Group 3–specific long noncoding RNA, *lnc-HLX-2-7*, in an in silico analysis of 175 MBs and confirmed its expression in Group 3 MB cell lines, patient-derived xenografts, and formalin-fixed paraffin-embedded samples. Knockdown of *lnc-HLX-2-7* significantly reduced cell growth and induced apoptosis. Deletion of *lnc-HLX-2-7* in cells injected into mouse cerebellums reduced tumor growth compared with parental cells, and bulk and single-cell RNA-seq of these tumors revealed *lnc-HLX-2-7*-associated modulation of cell viability, cell death, and energy metabolism signaling pathways. The *MYC* oncogene regulated *lnc-HLX-2-7*, and its expression was reduced by JQ1. *Lnc-HLX-2-7* is a candidate biomarker and a potential therapeutic target in Group 3 MBs.

Medulloblastoma (MB) is the most common malignant pediatric brain tumor.[1] Recent large-scale and high-throughput analyses have subclassified MBs into 4 molecularly distinct subgroups, each characterized by specific developmental origins, molecular features, and prognoses.[1–4] The well-characterized WNT and SHH subgroups have been causally linked to activated wingless and sonic hedgehog developmental cascades, respectively.[1] However, significant gaps remain in our understanding of the signaling pathways underlying Group 3 and Group 4 MBs, which account for 60% of all diagnoses and are frequently metastatic at presentation (~40%).[4] Group 3 and Group 4 tumors display significant clinical and genetic overlap, including similar location and presence of isochromosome 17q, and identifying these subgroups can be challenging without the application of multigene expression or methylation profiling. Therefore, improved understanding of Group 3 tumor drivers and theranostic targets is urgently needed.

The vast majority of the genome serves as a template for not only coding RNAs but also noncoding RNAs (ncRNAs). Of the noncoding RNAs, long noncoding RNAs (lncRNAs), which describe a class of RNAs >200 nucleotides in length, have been widely investigated and identified as key regulators of various biological processes, including cellular proliferation, differentiation, apoptosis, migration, and invasion.[5–8] LncRNAs are functionally diverse and participate in transcriptional silencing,[9] function as enhancers,[10] and sequester miRNAs from their target sites.[11] LncRNAs can also act as hubs for protein-protein and protein–nucleic acid interactions.[12] There is now a considerable body of evidence implicating lncRNAs in both health and disease, not least human tumorigenesis.[8,13,14] It has recently been reported that various lncRNAs play important roles in MB biology,[2,15–18] although the functional significance of many remains uncertain. Since many lncRNAs are uniquely expressed in specific cancer types,[19] they may function as powerful MB subgroup-specific biomarkers and therapeutic targets.

By analyzing RNA sequencing data derived from human MBs, here we report that the novel lncRNA *lnc-HLX-2-7* differentiates Group 3 from other MBs. Deletion by clustered regularly interspaced short palindromic repeat (CRISPR)/CRISPR associated protein (CRISPR/Cas9) of *lnc-HLX-2-7* in Group 3 MB cells significantly reduced cell growth in vitro and in vivo. RNA sequencing of xenografts revealed *lnc-HLX-2-7*–associated modulation of cell viability and cell death signaling pathways. *Lnc-HLX-2-7* is a promising novel biomarker and potential therapeutic target for Group 3 MBs.

Materials and Methods

MB Tissue and RNA Samples

Eighty MB tissue samples obtained from a tumor database maintained by the Department of Pathology at the Johns Hopkins Hospital were analyzed (Supplementary Table 1) under institutional review board (IRB) approved protocol NA_00015113. Detailed information about the RNA samples are described in the Supplementary Methods.

Patient In Silico Data

Raw FASTQ files for RNA sequencing data corresponding to 175 MB patients (referred to as the ICGC dataset) belonging to the 4 MB subgroups (accession number EGAS00001000215) were downloaded from the European Genome-Phenome Archive (EGA, http://www.ebi.ac.uk/ega/) after obtaining IRB approval.[20]

Cell Culture

Cell lines were authenticated using single tandem repeat profiling. D425 Med cells were cultured in DMEM/F12 with 10% serum and 1% glutamate/penicillin/streptomycin. MED211 cells were cultured in medium composed of 30% Ham's F12/70% DMEM, 1% antibiotic antimycotic, 20% B27 supplement, 5 µg/mL heparin, 20 ng/mL epidermal growth factor (EGF), and 20 ng/mL fibroblast growth factor 2. DAOY cells were cultured in DMEM with 10% serum and 1% glutamate/penicillin/streptomycin. All cells were grown in a humidified incubator at 37°C, 5% CO_2. For blocking of **bromodomain** and extraterminal domain family (BET) bromodomain protein in D425 Med and MED211 cells, Jun Qi 1 (JQ1) (SML1524-5MG, Sigma Aldrich) was added, and the medium was changed every other day.

Quantitative Real-Time PCR

Total RNA was purified using the Direct-zol RNA Miniprep kit (Zymo Research). To obtain RNA from xenografts, tumor tissues were pulverized and then used for purification. Quantitative PCR was carried out using SYBR Green mRNA assays as previously described.[8] Primer sequences are listed in Supplementary Table 2.

Antisense Oligonucleotides Lnc-HLX-2-7

Antisense oligonucleotides (ASOs) were designed using the Integrated DNA Technologies (IDT) Antisense Design Tool (IDT). ASO knockdowns were performed with 50 nM (final concentration) locked nucleic acid (LNA) GapmeRs transfected with Lipofectamine 3000 (Thermo Fisher Scientific). All ASOs were modified with phosphorothioate (PS) linkages. The following ASOs were used: ASO targeting *lnc-HLX-2-7* (ASO-*lnc-HLX-2-7*): +T*+G*+A*G*A*G*A*T*T*A*A*T*C*T*A*G*A*T*+T*+G*+C and control ASO targeting *luciferase* (ASO-*Luc*): +T*+C*+G*A*A*G*T*A*C*T*C*A*G*C*G*T*A*A*+G*+T*+T. The PS linkages are indicated with * and LNA-modified oligonucleotides are indicated with +.

SiRNA-Mediated Knockdown of HLX, MYC, and MYCN

Small interfering (si)RNAs targeting *HLX* (catalog no. 4427037, ID: s6639) and *MYC* (catalog no. 4427037, ID: s9129) were purchased from Thermo Fisher Scientific. SiRNAs were transfected at 20 nM for 48 h using Lipofectamine RNAiMAX (Thermo Fisher Scientific). The efficiency was determined by quantitative real-time (qRT)-PCR.

Cell Proliferation, Apoptosis, and 3D Colony Formation Assays

Cells were plated in 96-well plates at 5×10^3 cells per well in triplicate. After 72 hours of ASO or siRNA transfection, living cells were counted by trypan blue staining. Apoptotic cells were analyzed using a GloMax luminometer (Promega) with conditions optimized for the Caspase-Glo 3/7 Assay. For the 3D colony formation assay, cells were seeded in 24-well plates at a density of 1×10^2 cells/well and were stained with crystal violet solution approximately 14 days later. Colony number was determined using the EVE cell counter (Nano Entek), and staining intensity was analyzed using ImageJ software.

Lnc-HLX-2-7 CRISPR/Cas9 Knockdown in D425 Med Cells

The single guide RNA (sgRNA) targeting *lnc-HLX-2-7* was designed using Zhang Lab resources (http://crispr.mit.edu/) and synthesized to make the lenti-*lnc-HLX-2-7*-sgRNA-Cas9 constructs as described previously.[21] The DNA sequences for generating sgRNA were forward: 5′- GGACCCACTCTCCAACGCAG -3′ and reverse: 5′- GCAGGGACCCCTCATTGACG -3′. For the control plasmid, no sgRNA sequence was inserted into the construct. *Lnc-HLX-2-7*–edited cells and control cells were selected using 4 μg/mL puromycin. To determine the genome editing effect, total RNA was extracted from the *lnc-HLX-2-7*–edited cells and control cells and the expression of *lnc-HLX-2-7* quantified by qRT-PCR.

Medulloblastoma Xenografts (Intracranial)

All mouse studies were approved and performed in accordance with the policies and regulations of the Animal Care and Use Committee of Johns Hopkins University. Intracranial MB xenografts were established by injecting D425 Med cells, MED211 cells, D425 Med cells with *lnc-HLX-2-7* deleted, and MED211 cells with *lnc-HLX-2-7* deleted into the cerebellums of NOD-SCID mice (Jackson Laboratory). Cerebellar coordinates were –2 mm from lambda, +1 mm laterally, and 1.5 mm deep. Seven days after injection, mice were administered JQ1 (50 mg/kg) or vehicle alone (DMSO) on alternating days via intraperitoneal injection for 14 days. Tumor growth was evaluated by weekly bioluminescence imaging using an in vivo spectral imaging system (IVIS Lumina II, Xenogen).

Immunohistochemistry

For the analysis of cell proliferation, tumor sections were incubated with anti-Ki67 (Alexa Fluor 488 Conjugate) antibodies (#11882, 1:200, Cell Signaling Technology) at 4°C overnight. For the analysis of apoptosis, DeadEnd Fluorometric TUNEL System (Promega) was performed on the tumor sections, according to the manufacturer's instructions. The stained sections were imaged using a confocal laser-scanning microscope (Nikon C1 confocal system; Nikon). The acquired images were processed using the NIS (Nikon) and analyzed with ImageJ software (https://imagej.nih.gov/ij/).

Chromatin Immunoprecipitation

Cells (1×10^6) were treated with 1% formaldehyde for 8 minutes to crosslink histones to DNA. The cell pellets were resuspended in lysis buffer (1% sodium dodecyl sulfate, 10 mmol/L EDTA, 50 mmol/L Tris-HCl pH 8.1, and protease inhibitor) and sonicated using a Covaris S220 system. After diluting the cell lysate 1:10 with dilution buffer (1% Triton-X, 2 mmol/L EDTA, 150 mmol/L NaCl, 20 mmol/L Tris-HCl pH 8.1), diluted cell lysates were incubated for 16 h at 4°C with Dynabeads Protein G (100-03D, Thermo Fisher Scientific) precoated with 5 μL of anti-MYC antibody (ab32, Abcam). Chromatin immunoprecipitation (ChIP) products were analyzed by SYBR Green ChIP-qPCR using the primers listed in Supplementary Table 2.

RNA Library Construction and Sequencing

Total RNA was prepared from cell lines and orthotopic xenografts using Direct-zol RNA Miniprep kits (Zymo

Research). RNA quality was determined with the Agilent 2100 Bioanalyzer Nano Assay (Agilent Technologies). Using a TruSeq Stranded Total RNA library preparation Gold kit (Illumina), strand-specific RNA-seq libraries were constructed as per the instructions. The quantification and quality of final libraries were determined using KAPA PCR (Kapa Biosystems) and a high-sensitivity DNA chip (Agilent Technologies), respectively. Libraries were sequenced on an Illumina NovaSeq 6000 using 1 × 50 base paired-end reads. Detailed methods of sequence and data analysis are described in Supplementary Methods.

Ingenuity Pathway Analysis

To analyze pathways affected by *lnc-HLX-2-7*, differentially expressed genes between D425 Med and D425 Med with *lnc-HLX-2-7* deleted were compiled and analyzed using Qiagen Ingenuity Pathway Analysis (IPA). Analysis was conducted via the IPA web portal (www.ingenuity.com).

Data Availability

RNA-seq data described in the manuscript are accessible at NCBI GEO accession number GSE151810 and GSE156043.

RNA Fluorescence In Situ Hybridization

RNA was visualized in paraffin-embedded tissue sections using the QuantiGene ViewRNA ISH Tissue Assay Kit (Affymetrix). In brief, tissue sections were rehydrated and incubated with proteinase K. Subsequently, they were incubated with ViewRNA probesets designed against human *lnc-HLX-2-7*, *MYC*, and *MYCN* (Affymetrix). Custom type 1 primary probes targeting *lnc-HLX-2-7*, type 6 primary probes targeting *MYC*, and type 6 primary probes targeting *MYCN* were designed and synthesized by Affymetrix (Supplementary Table 2). Hybridization was performed according to the manufacturer's instructions.

Statistical Analysis

Statistical analyses were performed using GraphPad Prism software and the Limma R package. Data are presented as mean ± SD of 3 independent experiments. Differences between 2 groups were analyzed by the paired Student's *t*-test and correlations with the Pearson correlation coefficient. Kruskal–Wallis analysis was used to evaluate the differences between more than 2 groups. Survival analysis was performed using the Kaplan–Meier method and compared using the log-rank test.

Results

Identification of the Group 3–Specific Long-Noncoding RNA, lnc-HLX-2-7

To identify MB Group 3–specific lncRNAs, we obtained 175 RNA-seq files (FASTq) representing the 4 MB subgroups (WNT, SHH, Group 3, and Group 4) from the EGA and applied combined GENCODE and LNCipedia annotations.[22] Given the need to find novel biomarkers that differentiate Group 3 from other groups, we identified a set of lncRNAs (*lnc-HLX-1*, *lnc-HLX-2*, *lnc-HLX-5*, and *lnc-HLX-6*) with markedly elevated and significant overexpression in Group 3 MB (Fig. 1A, B and Supplementary Table 3). *Lnc-HLX-1*, *lnc-HLX-2*, *lnc-HLX-5*, and *lnc-HLX-6* showed a high expression correlation (Fig. 1C) and were highly expressed in Group 3 MB patient samples compared with other subgroups ($P < 0.01$; Fig. 1D). We recently reported that some of these lncRNAs also show Group 3–specific differential expression.[23] Due to *lnc-HLX-2*'s proximity to its host coding gene transcription factor and homeobox gene *HB24* (*HLX*) and a recent study reporting that the *lnc-HLX-2* region is a Group 3 MB–specific enhancer region (Supplementary Figure 1),[24] we focused on *lnc-HLX-2*. *Lnc-HLX-2* is located 2300 bp downstream of the transcriptional start site (TSS) of *HLX* (Supplementary Figure 2A) and consists of 11 transcripts (*lnc-HLX-2-1* to *lnc-HLX-2-11*; Supplementary Figure 2B), of which *lnc-HLX-2-7* was highly expressed in Group 3 MBs (Supplementary Figure 2C). Quantitative RT-PCR analysis verified that *lnc-HLX-2-7* was highly upregulated in Group 3 MB cell lines (Fig. 1E) and patient-derived xenograft (PDX) samples (Fig. 1F) compared with other groups. It was recently shown through a combined analysis of Group 3 and 4 MBs that they can be further subdivided into 8 molecular subtypes, designated I to VIII.[20] In a combined analysis of Group 3 and Group 4 cases, *lnc-HLX-2-7* showed high expression in subtype II and III MBs compared with other subtypes (Supplementary Figure 2D).

Lnc-HLX-2-7 Functions as an Oncogene In Vitro

To investigate the function of *lnc-HLX-2-7*, we used ASOs to inhibit *lnc-HLX-2-7* expression in D425 Med and MED211 MB cells. Transfection with ASO-*lnc-HLX-2-7* significantly decreased *lnc-HLX-2-7* expression compared with controls (ASO-Luc) in both cell lines ($P < 0.01$; Fig. 2A), which significantly suppressed MB cell growth and induced apoptosis ($P < 0.01$; Fig. 2B, C). Next, CRISPR/Cas9 knock-down was used to generate single-cell colonies and further investigate the effect of *lnc-HLX-2-7* in MB cells. We generated stable D425 Med and MED211-*lnc-HLX-2-7*-sgRNA cells, which constitutively expressed sgRNAs against *lnc-HLX-2-7* to reduce *lnc-HLX-2-7* expression (Fig. 2D). As expected, D425 Med and MED211-*lnc-HLX-2-7*-sgRNA cells showed reduced growth (Fig. 2E) and colony-forming ability (Fig. 2F) compared with D425 Med and MED211 control cells in vitro.

While the functions of the majority of lncRNAs are not yet known, some have been shown to function *in cis* by regulating the expression of neighboring genes.[25–27] Since *lnc-HLX-2-7* is located downstream of the *HLX* TSS (Supplementary Figure 2A), we determined whether *lnc-HLX-2-7* regulates *HLX* expression; indeed, *HLX* expression was significantly reduced in D425 Med and MED211 cells following treatment with ASO-*lnc-HLX-2-7* (Supplementary Figure 3). In addition, *HLX* knock-down significantly decreased the growth of D425 Med and MED211 cells (Supplementary Figure 4). While the current study focuses on the role of lncRNA *HLX-2-7*,

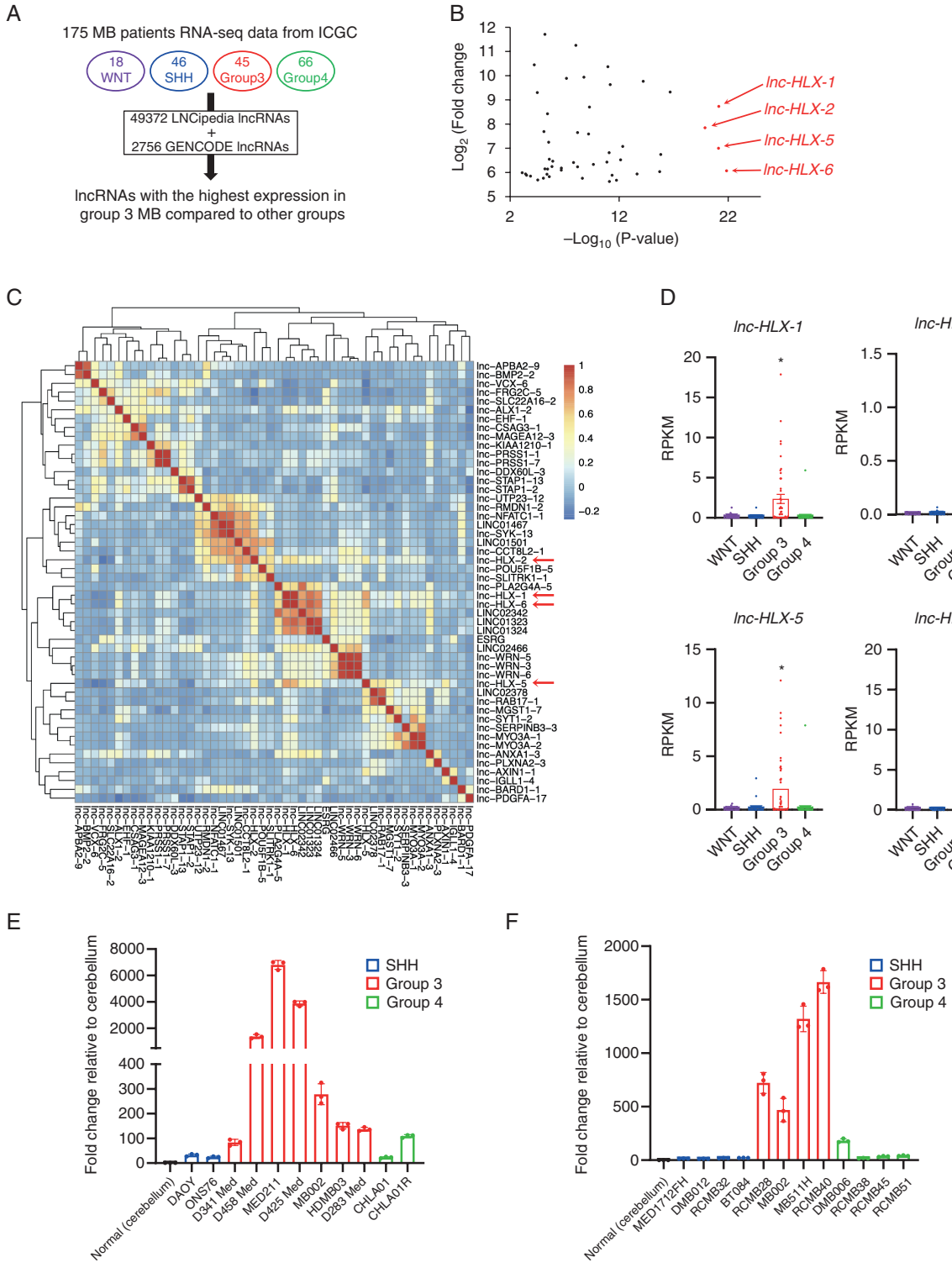

Fig. 1 Identification and validation of the Group 3–specific lncRNA, *lnc-HLX-2-7*. (A) Schematic of the identification of Group 3–specific lncRNAs in the 4 MB subgroups (WNT, SHH, Group 3 and Group 4). (B) Top 50 lncRNAs with the highest expression in Group 3 MBs compared with other MB subgroups are shown. x-axis indicates *P* value (-log10) of each lncRNA and y-axis indicates fold change value (log2) of each lncRNA. (C) The heat map represents the similarity of expression within Group 3 MBs of each lncRNA shown in (B). (D) Boxplot showing distribution of normalized expression values of *lnc-HLX-1*, *lnc-HLX-2*, *lnc-HLX-5*, and *lnc-HLX-6* in WNT, SHH, Group 3 and Group 4 MBs. Dots represent the expression value for each MB patient. **P* < 0.01, Kruskal–Wallis analysis. (E, F) qRT-PCR analysis showing the distribution of normalized expression values of *lnc-HLX-2-7* in MB cell lines (E) and PDX samples (F) of Group 3, Group 4, and SSH MBs. Values indicate fold change relative to cerebellum.

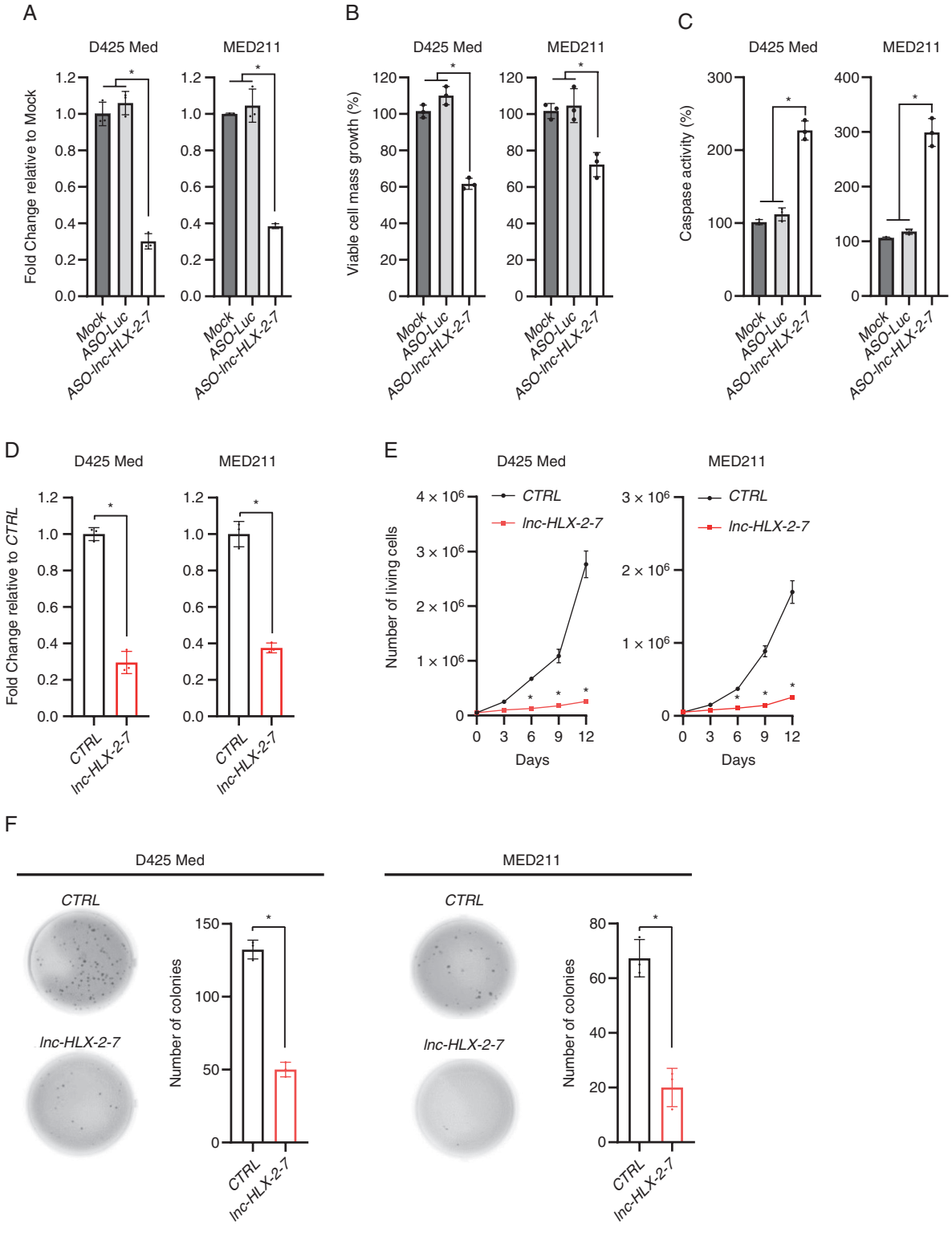

Fig. 2 Effects of *lnc-HLX-2-7* expression on the proliferation and apoptosis of Group 3 MB cells. (A) Expression level of *lnc-HLX-2-7* in D425 Med and MED211 cells treated with ASO against the genes indicated on the x-axis. Relative expression level to mock (non-transfected) is indicated on the y-axis. *$P < 0.01$, Kruskal–Wallis analysis. Viable cell numbers (B) and apoptotic cell numbers (C) in D425 Med and MED211 cells treated with either ASO-luc or ASO- *lnc-HLX-2-7*. Relative value to mock is indicated on the y-axis. *$P < 0.01$, Kruskal–Wallis analysis. (D) Expression level of *lnc-HLX-2-7* in D425 Med and MED211 control (*CTRL*) and D425 Med and MED211-*lnc-HLX-2-7*-sgRNA (*lnc-HLX-2-7*)

understanding the molecular function of its host-coding gene *HLX* requires further investigation, which is ongoing.

Lnc-HLX-2-7 Regulates Tumor Formation in Mouse Intracranial Xenografts

To evaluate the effect of *lnc-HLX-2-7* on tumor growth in vivo, we established intracranial MB xenografts in NOD-SCID mice. D425 Med and MED211 control cells and D425 Med and MED211-*lnc-HLX-2-7*-sgRNA cells were pre-infected with a lentivirus containing a luciferase reporter. Weekly evaluation of tumor growth by bioluminescence imaging revealed significantly smaller tumors in mice transplanted with D425 Med and MED211-*lnc-HLX-2-7*-sgRNA cells compared with mice transplanted with control cells ($n = 9$, $P < 0.05$; Fig. 3A, B). At day 30, tumors were harvested and cut into sections and then subjected to Ki67 and TUNEL staining. Ki67 analysis showed reduced cell proliferation in D425 Med-*lnc-HLX-2-7*-sgRNA cell-transplanted mice ($P < 0.01$; Fig. 3C). TUNEL analysis found out that *lnc-HLX-2-7* depletion induced significantly higher percentage of TUNEL-positive cells than compared with mice transplanted with control cells ($P < 0.01$; Fig. 3D). Kaplan–Meier plots demonstrated that the group transplanted with D425 Med and MED211-*lnc-HLX-2-7*-sgRNA cells had significantly prolonged survival compared with the control (Fig. 3E). Together, these results demonstrate that *lnc-HLX-2-7* regulates tumor growth in vivo and may function as an oncogene.

Transcriptional Regulation of lnc-HLX-2-7 by the MYC Oncogene

Since the majority of Group 3 tumors exhibit elevated expression and amplification of the *MYC* oncogene,[2,28] we hypothesized that MYC may regulate the expression of *lnc-HLX-2-7*. We therefore knocked down *MYC* by siRNA in D425 Med and MED211 cells, which decreased the expression of both *MYC* and *lnc-HLX-2-7* (Fig. 4A), suggesting that MYC may be an upstream regulator of *lnc-HLX-2-7*. To further support this, we also identified a MYC-binding motif (E-box; -*CACGTG*-) 772 bp upstream of the putative TSS of *lnc-HLX-2-7* using the JASPAR CORE database (http://jaspar.genereg.net/)[29] (Fig. 4B). To test whether MYC could interact with the endogenous *lnc-HLX-2-7* promoter, ChIP was performed in D425 Med and MED211 cells. ChIP analysis revealed that MYC bound to the E-box motif within the upstream region of *lnc-HLX-2-7* in D425 Med and MED211 cells, but not in DAOY cells (Fig. 4C). These results strongly suggest that MYC is a direct regulator of *lnc-HLX-2-7*.

JQ1 Regulates lnc-HLX-2-7 via MYC

Several previous studies have demonstrated that BRD4, a member of the bromodomain and extraterminal domain (BET) family, regulates *MYC* transcription and that JQ1 effectively suppresses cancer cell proliferation by inhibiting BRD4-mediated regulation of MYC in various types of cancer including MB.[30–34] To test the JQ1 effect on *lnc-HLX-2-7* regulation, we treated D425 Med and MED211 cells with different doses (100 or 300 nM) of the drug. As shown in Fig. 4D, both *MYC* and *lnc-HLX-2-7* were downregulated in D425 Med and MED211 cells. In addition, downregulation of *lnc-HLX-2-7* by JQ1 was also confirmed in vivo (Supplementary Figure 5). Interestingly, overexpression of *lnc-HLX-2-7* suppressed cell growth inhibition and downregulation of *MYC* by JQ1 (Supplementary Figure 6). Collectively, our results show that BRD4 inhibitors can be used to target MYC-mediated regulation of *lnc-HLX-2-7* expression.

RNA Sequencing Detects lnc-HLX-2-7 Interacting Genes and Pathways in Group 3 MBs

To gain further insights into the functional significance of *lnc-HLX-2-7*, gene expression was measured by RNA-seq in D425 Med-*lnc-HLX-2-7*-sgRNA cells and in xenografts derived from them. Among 1033 genes with a significant change in expression (false discovery rate [FDR] < 0.05), 484 genes were upregulated and 549 genes were downregulated in cultured D425 Med-*lnc-HLX-2-7*-sgRNA cells (Supplementary Figure 7A). IPA revealed that *lnc-HLX-2-7* knockdown preferentially affected genes associated with cell death (Supplementary Figure 7B). Of note, upstream regulator analysis showed that these genes contribute to important cancer pathways, including MYC, KRAS, HIF1A, and EGFR signaling (Supplementary Figure 7C). In xenografts, among 540 genes with a significant change in expression (FDR < 0.05), 409 genes were upregulated and 131 genes were downregulated (Fig. 5A). Differentially expressed genes detected by RNA-seq and pathway analysis were validated by qRT-PCR (Supplementary Figure 8). IPA analysis revealed that *lnc-HLX-2-7* knockdown preferentially regulated genes associated with cell viability (Fig. 5B). Canonical IPA pathway analysis showed that the pathways involved in important energy metabolism (oxidative phosphorylation, mitochondrial dysfunction, and sirtuin signaling pathways) were highly modulated by *lnc-HLX-2-7* (Fig. 5C and Supplementary Table 4).

Xenograft tumors were further characterized by single-cell RNA-seq. Subsequent to quality control, 3442 and 6193 single cells were obtained for D425 and *lnc-HLX-2-7* deleted D425 respectively (Supplementary Figure 9). Integrated

cells. Relative expression level to *CTRL* is indicated on the y-axis. *$P < 0.01$, Student's *t*-test. (E) Cell viability assays performed with D425 Med and MED211 control (*CTRL*) and D425 Med and MED211-*lnc-HLX-2-7*-sgRNA (*lnc-HLX-2-7*) cells. Points represent the mean and standard deviation of 3 biological replicates. *$P < 0.01$, Student's *t*-test. (F) Colony formation assays performed with D425 Med and MED211 control (*CTRL*) and D425 Med and MED211-*lnc-HLX-2-7*-sgRNA (*lnc-HLX-2-7*) cells. 3 independent experiments were performed, and data are presented as mean ± SD. *$P < 0.01$, Student's *t*-test.

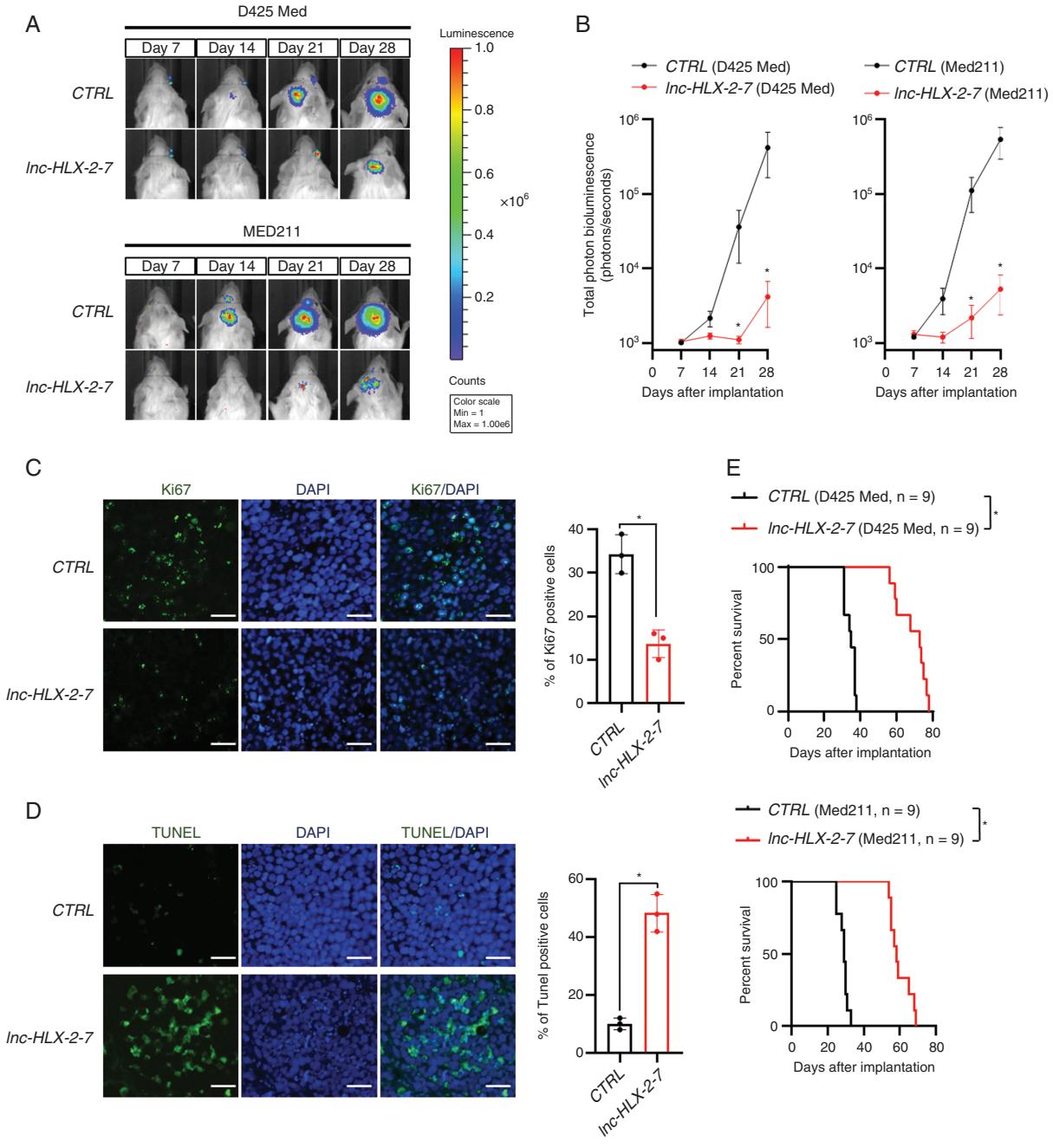

Fig. 3 *Lnc-HLX-2-7* promotes the tumorigenicity of Group 3 MB cells in vivo. (A) D425 Med and MED211 control (*CTRL*) and D425 Med- and MED211-*Inc-HLX-2-7*-sgRNA (*Inc-HLX-2-7*) cells expressing luciferase were implanted into the right forebrains of NOD-SCID mice, and tumor formation was assessed by bioluminescence imaging. Changes in bioluminescent signal were examined weekly after tumor implantation. (B) Quantification of total photon counts from mice implanted with D425 Med and MED211 control (*CTRL*) and D425 Med- and MED211-lnc-HLX-2-7-sgRNA (*Inc-HLX-2-7*) cells. $n = 9$, $^*P < 0.05$, Student's *t*-test. (C) Ki67 and (D) TUNEL staining of xenograft tumors. Nuclei are stained with DAPI. Scale bars, 50 μm. Quantification of Ki67 and TUNEL-positive cells were shown. $^*P < 0.05$, Student's *t*-test. (E) Overall survival was determined by Kaplan–Meier analysis, and the log-rank test was applied to assess the differences between groups. $^*P < 0.05$, Mantel–Cox log-rank test.

clustering of D425 control and *Inc-HLX-2-7* depleted xenografts resulted in 5 clusters of single cells (Fig. 5D). Clusters 1 and 2 were almost entirely from D425 control xenografts, while clusters 3, 4, and 5 were almost exclusively from *Inc-HLX-2-7* depleted xenografts (Fig. 5E). The top canonical pathways impacted in *Inc-HLX-2-7*-depleted single cell populations compared with D425 controls included the oxidative phosphorylation and sirtuin signaling pathways (Fig. 5F, Supplementary Tables 5, 6), consistent with the bulk RNA-seq data. Based on our earlier result that

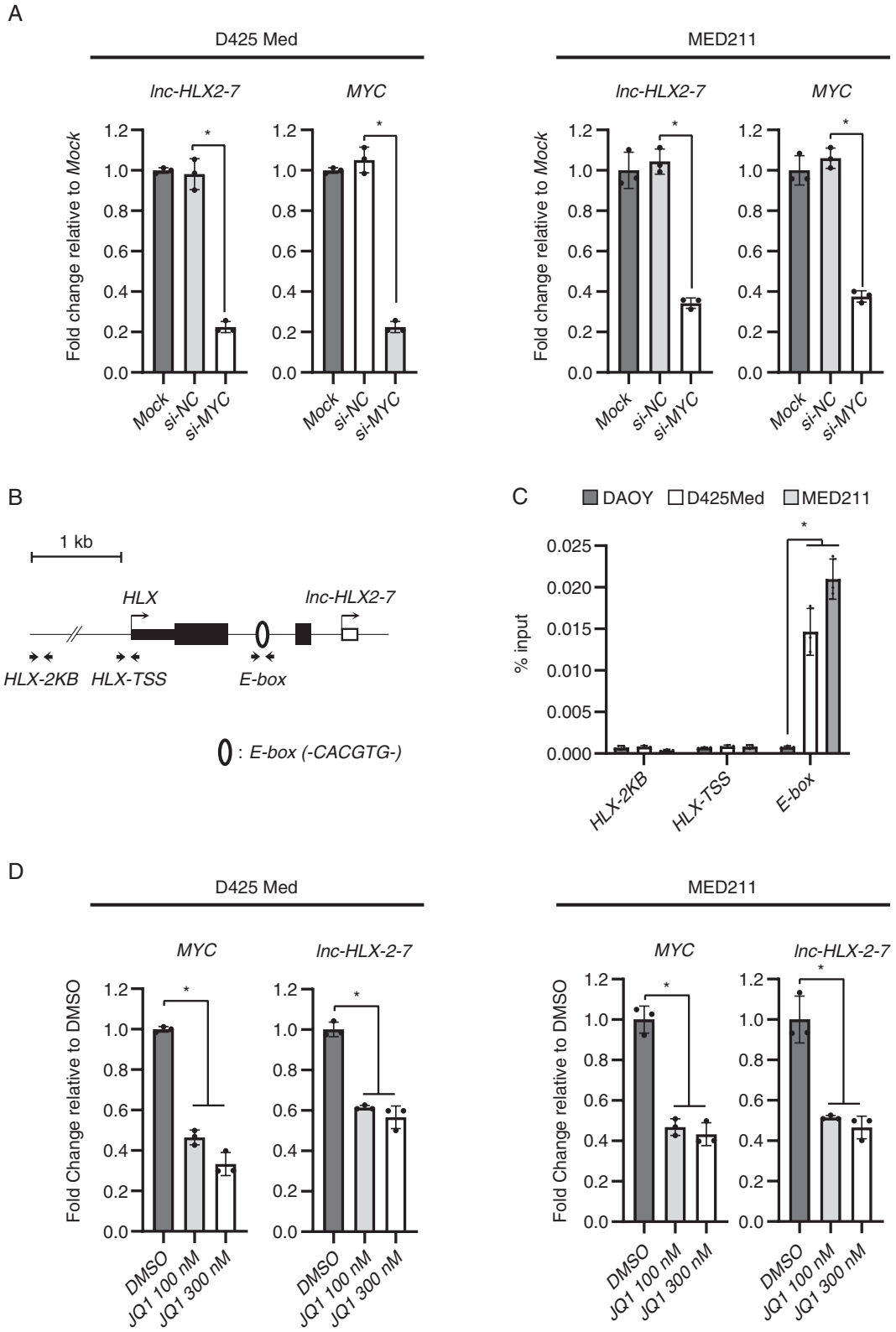

Fig. 4 MYC regulates the expression of *lnc-HLX-2-7* in Group 3 MB. (A) Expression levels of *MYC* and *lnc-HLX-2-7* in D425 Med and MED211 cells treated with siRNA against the indicated genes on the x-axis. Relative expression level to mock (non-transfected) is indicated on the y-axis. **P* < 0.01, Kruskal–Wallis analysis. (B) Schematic diagram showing E-box motifs around the TSS of *lnc-HLX-2-7*. Open circles indicate E-box motifs. Arrows show the primer location of ChIP-qPCR. (C) Enrichment of MYC in the *lnc-HLX-2-7* promoter regions in DAOY, D425 Med, and MED211 cells. Enrichment is expressed as a percentage of input DNA. **P* < 0.01, Student's *t*-test. (C) Expression level of *MYC* and *lnc-HLX-2-7* in D425 Med, and MED211 cells treated with JQ1. Values are indicated relative to abundance in DMSO-treated cells. **P* < 0.01, Kruskal–Wallis analysis.

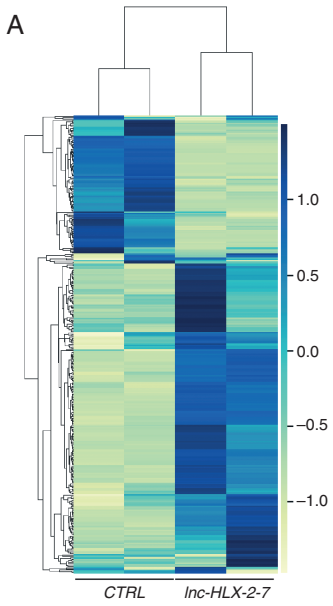

B

Diseases or Functions Annotation	p-value	Predicted Activation State	Activation z-score
Cell viability of cerebral cortex cells	0.00356	Inhibited	−0.804
Cell viability of cortical neurons	0.00385	Inhibited	−0.739
Cell viability of kidney cell lines	0.00307	Inhibited	−0.420

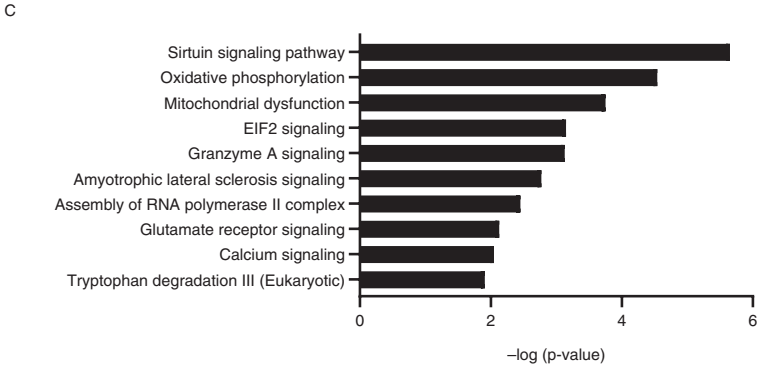

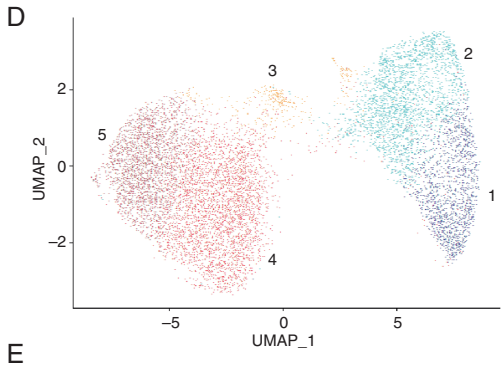

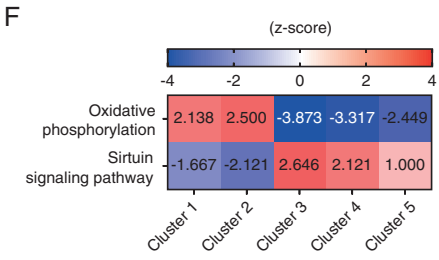

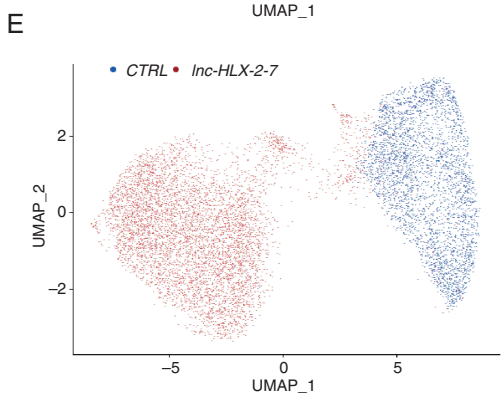

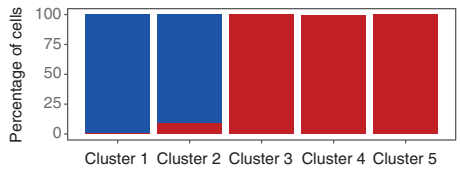

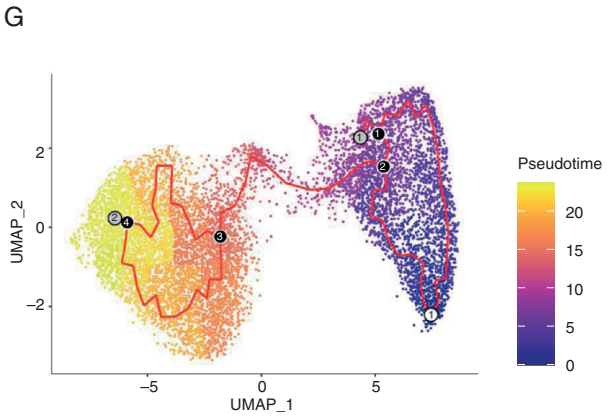

Fig. 5 RNA sequencing detects *lnc-HLX-2-7* interacting genes and pathways. (A) Heatmap representation of genes up and downregulated after *lnc-HLX-2-7* depletion in D425 xenografts. (B) Molecular and cellular functions and diseases associated with these genes. (C) IPA Canonical Pathway analysis was performed to predict signaling pathway activity. The 10 most significant pathways with lowest *P* values are presented. (D) Uniform Manifold Approximation and Projection (UMAP) plot of transcriptionally distinct cell populations from aggregate *CTRL*

D425 control and *lnc-HLX-2-7* depleted single cells form separate clusters, we performed pseudotemporal ordering of cells using Monocle3[35] to identify genes responsible for the transition from the D425 control to *lnc-HLX-2-7*-depleted state (Fig. 5G). A graph path corresponding to transition of cells from cluster 1 through 5 was observed (Supplementary Figure 10). The top 370 genes contributing to the cell transition were selected based on Moran's I and consisted of important genes involved in the development and malignancy of MB such as *MYC*, *SOX4*, *CDK6*, and *CHD7* (Supplementary Table 7).

Lnc-HLX-2-7 Expression Is Specific to Group 3 MBs

We next confirmed Group 3 specificity by visualizing *lnc-HLX-2-7* expression by RNA fluorescence in situ hybridization (FISH) in formalin-fixed paraffin-embedded tissue samples from D425 Med mouse xenografts and patients with MB. *Lnc-HLX-2-7* was expressed in D425 Med mouse xenografts but not normal brain (Supplementary Figure 11), and *lnc-HLX-2-7* was readily detected in all Group 3 MB samples but not in Group 4 MBs (Fig. 6A, B). Quantitative analysis of the tissues further confirmed significantly higher *lnc-HLX-2-7* expression in Group 3 MBs compared with Group 4 and SHH MBs with high sensitivity (95.0%) and specificity (95.0%, $n = 20$, $P < 0.01$; Fig. 6C and Supplementary Figure 12). Importantly, *lnc-HLX-2-7* expression was highly correlated with *MYC* expression in Group 3 MBs ($n = 20$, $P < 0.01$; Fig. 6D). This positive correlation between *lnc-HLX-2-7* and *MYC* expression in Group 3 MB was further validated in RNA-seq data from 175 MB patients (Supplementary Figure 13). Finally, *lnc-HLX-2-7* overexpression was associated with poor patient outcomes and mirrored that of *MYC* expression in Group 3 MB (Fig. 6E). Collectively, our analyses suggest that *lnc-HLX-2-7* expression is specific to Group 3 MBs and can be detected using an assay readily applicable to the clinical setting.

Discussion

The functions and clinical relevance of lncRNAs in MB are poorly described. Here we provide evidence that the lncRNA *lnc-HLX-2-7* is clinically relevant and biologically functional in Group 3 MBs. Using publicly available patient-derived RNA-seq datasets, we discovered that *lnc-HLX-2-7* expression is particularly high in Group 3 MBs compared with other groups. By depleting the expression of *lnc-HLX-2-7* by CRISPR/Cas9 and ASOs, we showed both in vitro and in vivo that *lnc-HLX-2-7* knockdown reduced proliferation and colony formation and increased apoptosis in MB.

The region encoded by *lnc-HLX-2-7* has been reported as a Group 3 MB–specific enhancer region.[24] Therefore, ncRNAs transcribed from this region may function as enhancer RNAs, a class of lncRNAs synthesized at enhancers, and may regulate the expression of their surrounding genes. We found that *lnc-HLX-2-7* positively regulated the expression of the adjacent *HLX* gene. Although the mechanism by which *lnc-HLX-2-7* regulates *HLX* remains unclear, *lnc-HLX-2-7* may function as an eRNA in this context. *HLX* has recently been shown to be a key gene mediating BET inhibitor responses and resistance in Group 3 MBs.[36] In this study, we discovered that *lnc-HLX-2-7* controls *HLX* expression and contributes to MB cell proliferation, so it is possible that it may influence BET inhibitor resistance. In addition, our results show that the *MYC* oncogene regulates *lnc-HLX-2-7* expression. A recent report suggests that the small molecule JQ1, a BET inhibitor that disrupts interactions with MYC, could be a therapeutic option to treat Group 3 MBs.[37] However, Group 3 MB tumors may also become resistant to BET inhibitor through mutations in the *BRD4* gene, and transcription factors like MYC and HLX are poor therapeutic targets with short half-lives and pleiotropic properties.[38] We postulate that *lnc-HLX-2-7* inhibition may provide a novel solution to BET inhibitor resistance or amplify the effects of BET inhibitors, a hypothesis that requires further investigation.

Recent evidence shows that HLX directly regulates several metabolic genes and controls mitochondrial biogenesis.[39] In the present study, we demonstrate that *lnc-HLX-2-7* modulated oxidative phosphorylation, mitochondrial dysfunction, and sirtuin signaling pathways in intracranial xenograft models. These findings suggest that *lnc-HLX-2-7* contributes to the metabolic state of Group 3 MBs by regulating HLX expression. This newly discovered link between *lnc-HLX-2-7* and metabolism may have important therapeutic implications.

Group 3 and Group 4 MBs display clinical and genetic overlap, with similar anatomic location and presence of isochromosome 17q, so it is not currently possible to distinguish them without applying multigene expression or methylation profiling. *Lnc-HLX-2-7* may represent a useful single molecular marker that could distinguish Group 3 from Group 4 MBs. Furthermore, RNA-FISH using probes targeting *lnc-HLX-2-7*, a technique readily applicable in clinical laboratories, readily discriminated Group 3 from Group 4 MBs. It was recently shown through a combined analysis of Group 3 and 4 MBs that they can be subdivided

and *lnc-HLX-2-7*-deleted xenograft scRNA-seq samples. Five distinct clusters (1-5) were identified. Marker genes associated with each cluster are listed in Supplementary Table 5. (E) UMAP plot with *CTRL* and *lnc-HLX-2-7*-deleted xenograft samples highlighted. Bar chart indicates the percentage of cells from each xenograft sample for the clusters corresponding to (D). (F) IPA Canonical Pathway analysis to predict signaling pathway activity in clusters 1, 2, 3, 4, and 5. The top canonical pathways with lowest adjusted *P* values are shown. (G) Pseudotemporal trajectory of cells from *CTRL* to *lnc-HLX-2-7*-deleted cells. Numbered circle with white background denotes the root node selected for pseudotemporal ordering, black circles represent branch nodes (where cells can proceed to different outcomes), and gray circles indicate different outcomes. The red trajectory denotes the structure of pseudotime graph. Cell colors denote the progression of cells along pseudotime.

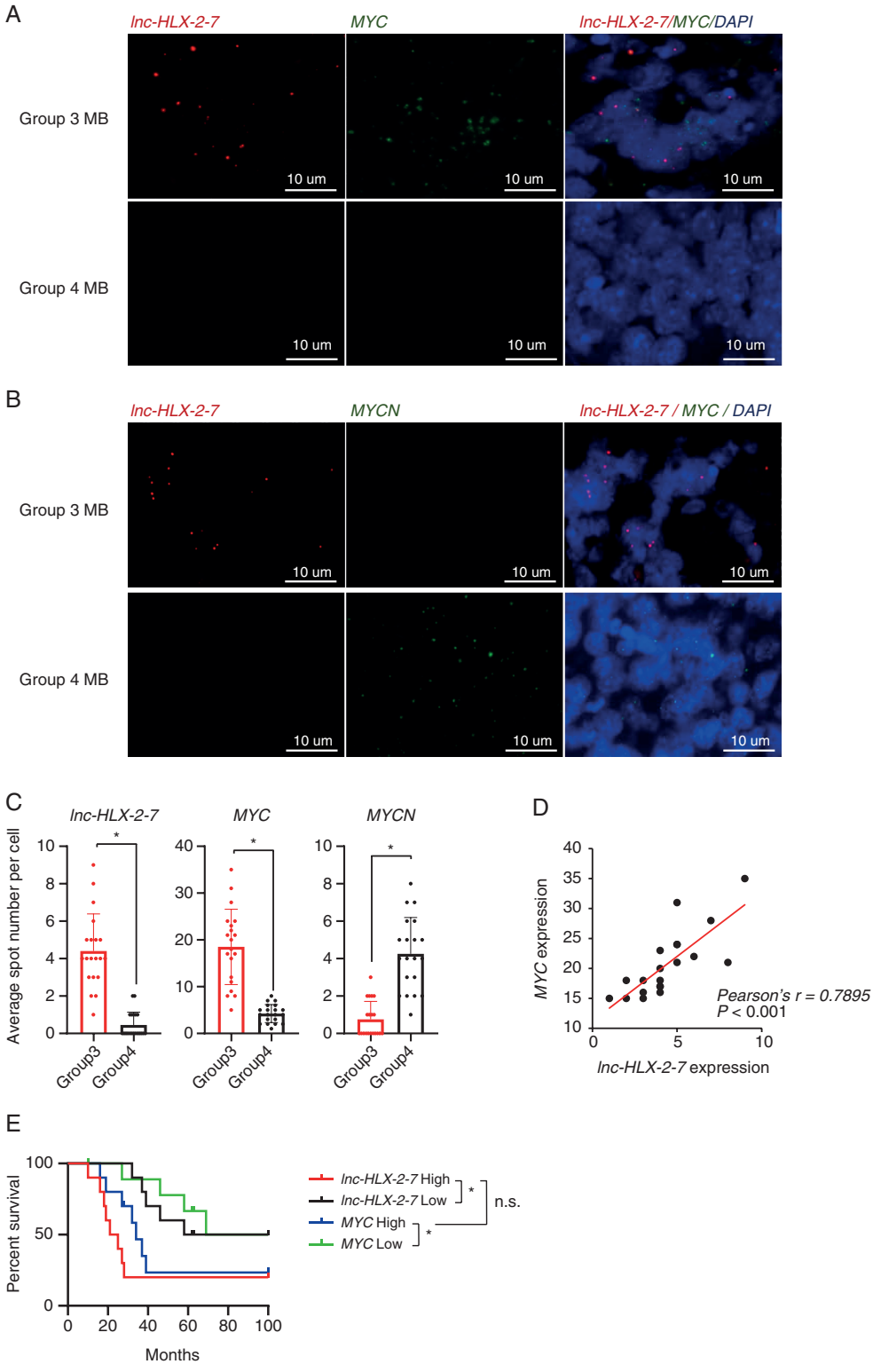

Fig. 6 RNA-FISH confirms that *lnc-HLX-2-7* expression is specific to Group 3 MB patients. (A) Representative RNA-FISH analysis of *lnc-HLX-2-7* and *MYC* in MB tissues. RNA-FISH analysis of *lnc-HLX-2-7* and *MYC* in Group 3 MB patients (upper panels) and Group 4 MB patients (lower panels). (B) Representative RNA-FISH analysis of *lnc-HLX-2-7* and *MYCN* in MB tissues. RNA-FISH analysis of *lnc-HLX-2-7* and *MYCN* in Group 3 MB patients (upper panels) and Group 4 MB patients (lower panels). Nuclei are stained with DAPI. Scale bars, 10 μm. (C) The spot numbers relating to *lnc-HLX-2-7*, *MYC*, and *MYCN* were quantified per cell in Group 3 and Group 4 MB patients. $n = 20$, $^*P < 0.01$, Student's *t*-test. (D) Correlation between *lnc-HLX-2-7* and *MYC* expression in Group 3 MB patients. $n = 20$, $^*P < 0.01$, Pearson correlation coefficient. (E) Kaplan–Meier survival curves of Group 3 MB patients according to *lnc-HLX-2-7* and *MYC* expression. $n = 10$, $^*P < 0.01$, log-rank test.

into 8 molecular subtypes, designated I to VIII.[20] Subtypes II and III are characterized by amplification of the *MYC* oncogene and are associated with the poorest prognosis.[40] We found that *Inc-HLX-2-7* is specifically expressed in subtype II and III MBs. These findings strongly suggest that *Inc-HLX-2-7* may be an ideal prognostic marker in Group 3 MBs.

In conclusion, we show that the lncRNA *Inc-HLX-2-7* is clinically and functionally relevant in Group 3 MBs. Future studies will determine the mechanism by which *Inc-HLX-2-7* promotes MB tumorigenesis. Together, our findings support the hypothesis that lncRNAs, and *Inc-HLX-2-7* in particular, are functional in human MBs and may offer promising future opportunities for diagnosis and therapy.

Supplementary Material

Supplementary data are available at *Neuro-Oncology* online.

Keywords

medulloblastoma | *Inc-HLX-2-7* | *MYC* | biomarker | therapeutic target

Funding

The Schamroth Project is funded by Ian's Friends Foundation to R.J.P, G.J., and C.B. The Hough Foundation grant to R.J.P and G.J. This study was also supported by P30 CA006973 (JHU SKCCC) to R.J.P. C.G.E, E.R., and C.B. and NCI 5P30CA030199 (SBP) to R.W-R. K.K. was supported by fellowship grants from the Uehara Memorial Foundation.

Acknowledgments

We thank Ms Tiffany Casey for helping us with the manuscript formatting. No unpublished data are referenced in this study.

Conflict of interest statement. The authors declare no conflicts of interest.

Authorship statement. K.K., B.L., and R.J.P. designed the study. K.K., B.L., and H.K. performed the experimental work. C.Z., B.L., R.M., and J.Y. performed data analyses. C.G.E., E.R., C.B., S.S., G.J., A.G., I.G., H.L.M., R.V., and R.W. provided cell lines, patient samples, TMAs, FFPE sections, and PDXs for the study. K.K., R.J.P., E.R., and C.G.E. wrote the main draft of the text. All authors revised and approved the final version of the manuscript.

References

1. Northcott PA, Jones DT, Kool M, et al. Medulloblastomics: the end of the beginning. *Nat Rev Cancer.* 2012;12(12):818–834.
2. Northcott PA, Shih DJ, Peacock J, et al. Subgroup-specific structural variation across 1,000 medulloblastoma genomes. *Nature.* 2012;488(7409):49–56.
3. Jones DT, Jäger N, Kool M, et al. Dissecting the genomic complexity underlying medulloblastoma. *Nature.* 2012;488(7409):100–105.
4. Taylor MD, Northcott PA, Korshunov A, et al. Molecular subgroups of medulloblastoma: the current consensus. *Acta Neuropathol.* 2012;123(4):465–472.
5. Wahlestedt C. Targeting long noncoding RNA to therapeutically upregulate gene expression. *Nat Rev Drug Discov.* 2013;12(6):433–446.
6. Schmitt AM, Chang HY. Long noncoding RNAs in cancer pathways. *Cancer Cell.* 2016;29(4):452–463.
7. Quinn JJ, Chang HY. Unique features of long noncoding RNA biogenesis and function. *Nat Rev Genet.* 2016;17(1):47–62.
8. Khaitan D, Dinger ME, Mazar J, et al. The melanoma-upregulated long noncoding RNA SPRY4-IT1 modulates apoptosis and invasion. *Cancer Res.* 2011;71(11):3852–3862.
9. Sahakyan A, Yang Y, Plath K. The role of Xist in X-chromosome dosage compensation. *Trends Cell Biol.* 2018;28(12):999–1013.
10. Trimarchi T, Bilal E, Ntziachristos P, et al. Genome-wide mapping and characterization of Notch-regulated long noncoding RNAs in acute leukemia. *Cell.* 2014;158(3):593–606.
11. Katsushima K, Natsume A, Ohka F, et al. Targeting the Notch-regulated noncoding RNA TUG1 for glioma treatment. *Nat Commun.* 2016;7:13616.
12. Long Y, Wang X, Youmans DT, Cech TR. How do lncRNAs regulate transcription? *Sci Adv.* 2017;3(9):eaao2110.
13. Esteller M. Noncoding RNAs in human disease. *Nat Rev Genet.* 2011;12(12):861–874.
14. Wapinski O, Chang HY. Long noncoding RNAs and human disease. *Trends Cell Biol.* 2011;21(6):354–361.
15. Varon M, Levy T, Mazor G, et al. The long noncoding RNA TP73-AS1 promotes tumorigenicity of medulloblastoma cells. *Int J Cancer.* 2019;145(12):3402–3413.
16. Joshi P, Katsushima K, Zhou R, et al. The therapeutic and diagnostic potential of regulatory noncoding RNAs in medulloblastoma. *Neurooncol Adv.* 2019;1(1):vdz023.
17. Zhang Y, Wang T, Wang S, et al. Nkx2-2as suppression contributes to the pathogenesis of sonic hedgehog medulloblastoma. *Cancer Res.* 2018;78(4):962–973.
18. Gao R, Zhang R, Zhang C, Zhao L, Zhang Y. Long noncoding RNA CCAT1 promotes cell proliferation and metastasis in human medulloblastoma via MAPK pathway. *Tumori.* 2018;104(1):43–50.
19. Iyer MK, Niknafs YS, Malik R, et al. The landscape of long noncoding RNAs in the human transcriptome. *Nat Genet.* 2015;47(3):199–208.
20. Northcott PA, Buchhalter I, Morrissy AS, et al. The whole-genome landscape of medulloblastoma subtypes. *Nature.* 2017;547(7663):311–317.
21. Lee B, Sahoo A, Marchica J, et al. The long noncoding RNA SPRIGHTLY acts as an intranuclear organizing hub for pre-mRNA molecules. *Sci Adv.* 2017;3(5):e1602505.
22. Uszczynska-Ratajczak B, Lagarde J, Frankish A, Guigó R, Johnson R. Towards a complete map of the human long non-coding RNA transcriptome. *Nat Rev Genet.* 2018;19(9):535–548.
23. Joshi P, Jallo G, Perera RJ. In silico analysis of long non-coding RNAs in medulloblastoma and its subgroups. *Neurobiol Dis.* 2020;141:104873.

24. Lin CY, Erkek S, Tong Y, et al. Active medulloblastoma enhancers reveal subgroup-specific cellular origins. *Nature.* 2016;530(7588):57–62.
25. Engreitz JM, Haines JE, Perez EM, et al. Local regulation of gene expression by lncRNA promoters, transcription and splicing. *Nature.* 2016;539(7629):452–455.
26. Joung J, Engreitz JM, Konermann S, et al. Genome-scale activation screen identifies a lncRNA locus regulating a gene neighbourhood. *Nature.* 2017;548(7667):343–346.
27. Toiber D, Leprivier G, Rotblat B. Long noncoding RNA: noncoding and not coded. *Cell Death Discov.* 2017;3:16104.
28. Cavalli FMG, Remke M, Rampasek L, et al. Intertumoral heterogeneity within medulloblastoma subgroups. *Cancer Cell.* 2017;31(6):737–754.e736.
29. Mathelier A, Wasserman WW. The next generation of transcription factor binding site prediction. *PLoS Comput Biol.* 2013;9(9):e1003214.
30. Bolin S, Borgenvik A, Persson CU, et al. Combined BET bromodomain and CDK2 inhibition in MYC-driven medulloblastoma. *Oncogene.* 2018;37(21):2850–2862.
31. Venkataraman S, Alimova I, Balakrishnan I, et al. Inhibition of BRD4 attenuates tumor cell self-renewal and suppresses stem cell signaling in MYC driven medulloblastoma. *Oncotarget.* 2014;5(9):2355–2371.
32. Henssen A, Thor T, Odersky A, et al. BET bromodomain protein inhibition is a therapeutic option for medulloblastoma. *Oncotarget.* 2013;4(11):2080–2095.
33. Shi X, Liu C, Liu B, Chen J, Wu X, Gong W. JQ1: a novel potential therapeutic target. *Pharmazie.* 2018;73(9):491–493.
34. Delmore JE, Issa GC, Lemieux ME, et al. BET bromodomain inhibition as a therapeutic strategy to target c-Myc. *Cell.* 2011;146(6):904–917.
35. Trapnell C, Cacchiarelli D, Grimsby J, et al. The dynamics and regulators of cell fate decisions are revealed by pseudotemporal ordering of single cells. *Nat Biotechnol.* 2014;32(4):381–386.
36. Bandopadhayay P, Piccioni F, O'Rourke R, et al. Neuronal differentiation and cell-cycle programs mediate response to BET-bromodomain inhibition in MYC-driven medulloblastoma. *Nat Commun.* 2019;10(1):2400.
37. Bandopadhayay P, Bergthold G, Nguyen B, et al. BET bromodomain inhibition of MYC-amplified medulloblastoma. *Clin Cancer Res.* 2014;20(4):912–925.
38. McKeown MR, Bradner JE. Therapeutic strategies to inhibit MYC. *Cold Spring Harb Perspect Med.* 2014;4(10).
39. Piragyte I, Clapes T, Polyzou A, et al. A metabolic interplay coordinated by HLX regulates myeloid differentiation and AML through partly overlapping pathways. *Nat Commun.* 2018;9(1):3090.
40. Sharma T, Schwalbe EC, Williamson D, et al. Second-generation molecular subgrouping of medulloblastoma: an international meta-analysis of Group 3 and Group 4 subtypes. *Acta Neuropathol.* 2019;138(2):309–326.